Check for updates

Designing a compact photonic crystal decoder using graphene-SiO$_2$ stack

M. Soroosh[1] · **M. Shahbaznia**[2] · **M. J. Maleki**[1] · **J. Ganji**[2]

© The Author(s), under exclusive licence to Springer Science+Business Media, LLC, part of Springer Nature 2024

Abstract

In this study, a novel approach is described for developing an electro-optic decoder utilizing a combination of photonic crystals and a graphene stack. The decoder structure comprises three main components: silicon waveguides, stacks, and one-dimensional photonic crystals. To create favorable interferences similar to reflectors based on Bragg layers, a one-dimensional array of air holes is designed in parallel with a waveguide. Within this array, a graphene-SiO$_2$ stack is incorporated, enabling the creation of a tunable stop-band frequency filter within the wavelength range of 1489 to 1492 nm. This tunability is achieved by altering the graphene refractive index according to the applied chemical potential. By controlling the optical wave transmission through the waveguides, the transmission from the input to the output ports is effectively regulated. Simulation results indicate that decoding operation can be achieved by applying chemical potentials of 0.1 eV and 0.9 eV. The normalized power levels for logic states 1 and 0 are equal to 48% and 6.2%, respectively, resulting in a contrast ratio of 8.89 dB. Additionally, the compact size of the designed structure, occupying only 99 μm^2 of space, demonstrates its advantages over previous electro-optic works, particularly in terms of realizing optical circuits.

1 Introduction

Researchers have been paying much attention to designing optical components due to the high need for ultra-fast processing (Osgood et al. 2021). In recent years, there have been numerous attempts to develop devices based on photonic crystals (PCs). These arrays, composed of dielectric materials, possess remarkable features such as photonic bandgap (Maleki et al. 2021a), slow light (Daghooghi et al. 2019), and self-collimation (Noori et

---

✉ M. Soroosh
  m.soroosh@scu.ac.ir

1   Department of Electrical Engineering, Shahid Chamran University of Ahvaz, Ahvaz, Iran

2   Department of Electrical Engineering, Mahshahr Branch, Islamic Azad University, Tehran, Iran

al. 2018). The low optical power requirement and high-speed response of photonic crystals make them ideal for optical switching and processing. Consequently, various PC-based devices including filters (Foroughifar et al. 2021; Hosseinzadeh Sani et al. 2020), logic gates (Askarian and Parandin 2023a; Parandin et al. 2021; Askarian 2022b; Mehdizadeh et al. 2016a), decoders (Daghooghi et al. 2019; Serajmohammadi et al. 2015; Alipour-Banaei et al. 2015; Mehdizadeh et al. 2016b; Moniem 2016; Khosravi et al. 2017; Daghooghi et al. 2017; Salimzadeh et al. 2018; Daghooghi et al. 2018a, b; Maleki et al. 2019, Maleki et al. 2020b; Maleki et al. 2020c; Askarian et al. 2022a; Rahmi et al. 2022; Maleki et al. 2023b; Arunkumar et al. 2023), encoders (Haddadan et al. 2019a; Mehdizadeh et al. 2017a; Haddadan et al. 2019b; Makvandi et al. 2020; Askarian 2023b; Haddadan et al. 2020), multiplexers (Maleki and Soroosh 2022a; Askarian 2021c; Maleki et al. 2022b), Comparators (Askarian 2021a; Askarian and Parandin 2023c), flip-flop (Parandin et al. 2024), and adders/subtractors (Maleki et al. 2020a, 2021b; Askarian et al. 2019; Askarian 2021b) have been proposed.

Optical waveguides play a crucial role in the design of optical devices as they enable light transmission through the incorporation of linear and nonlinear defects. Photonic crystal cavities, capable of guiding different modes, facilitate the interaction between light and matter, finding applications in fields such as quantum information processing, nonlinear optics, optical trapping, and optofluidics (Maleki et al. 2023a).

Researchers are currently highly interested in the use of new materials to attain a wide range of optical and electrical properties. One particularly appealing material in electro-optic applications is graphene, known for its tunability. By controlling the graphene chemical potential, conductivity, permittivity, and effective refractive index can be modified. Furthermore, graphene exhibits a rapid response to external fields, typically less than 10^{-13} seconds (Jonghwan et al. 2012). Xu et al. (2015) successfully approached an effective light-graphene interaction by using the resonance phenomenon in a photonic crystal structure. It was observed that employing multilayer graphene yielded stronger resonance and higher quality factors.

Numerous attempts have been made to develop decoders using photonic crystal structures (Daghooghi et al. 2019; Serajmohammadi et al. 2015; Khosravi et al. 2017; Salimzadeh et al. 2018; Alipour-Banaei et al. 2015; Moniem 2016; Mehdizadeh et al. 2016b; Daghooghi et al. 2018a, b). These devices effectively guide optical waves and transfer them between waveguides to enable the desired outputs for accurate decoding operations. The first PC-based decoder structure was proposed by Serajmohammadi et al. (2015), who designed a 1-to-2 decoder utilizing a ring resonator while considering nonlinear properties. The structure operated at a wavelength of approximately 1550 nm with an area of 267 µm². Alipour-Banaei et al. (2015) then presented an all-optical 2-to-4 decoder based on PCs, incorporating chalcogenide glass rods and three ring resonators within an area of 611.7 µm². Subsequently, Mehdizadeh et al. (2016b) introduced an all-optical 2-to-4 decoder plan utilizing a bias signal and five ring resonators within an area of 1823 µm². Moniem (2016) designed a decoder structure with two inputs using a square arrangement of PCs, employing five nonlinear ring resonators along with T-shaped waveguides and Y-shaped branches to guide the optical signals. The structure occupied an area of approximately 1520 µm².

A 2-to-4 decoder utilizing a square arrangement and three nonlinear ring resonators was reported by Khosravi and Zavari (2017). The contrast ratio was calculated at 3.37 dB, while the area covered by the structure was 1228 µm². Daghooghi et al. (2017) introduced a 2-to-4

decoder structure employing six nonlinear ring resonators. The contrast ratio achieved approximately 5.68 dB, and the normalized output power reached 38%. The decoder occupied a relatively large area of 1854.4 μm^2. In the realm of decoder design, Salimzadeh et al. (2018) reported a 3-to-8 decoder by combining seven 1-to-2 decoders, resulting in an enhanced contrast ratio of 9.29 dB through improved coupling efficiency. Daghooghi et al. (2018a) proposed a novel structure with fewer resonators, which yielded a contrast ratio of 9.95 dB while maintaining a smaller physical footprint compared to previous works. Moreover, in the slow-light regime, Daghooghi et al. (2019) proposed another decoder structure featuring nonlinear cavities. The device demonstrated a contrast ratio of 13.12 dB with an area of 228 μm^2.

Maleki et al. (2019; Maleki and Soroosh 2020b; Maleki et al. 2020c) reported three structures in which an optical signal was applied to the main waveguides. The signal was dropped through resonant cavities corresponding to the optical intensity into the waveguide. The amount of the optical intensity depends on the working states of the 2-to-4 decoder. The dropping operation was achieved by using nonlinear defects with different radii. Each resonant cavity was connected to an output port. Recently, they designed a new structure including four resonant cavities and changed the form of the main waveguide to improve the performance of PC-based decoders (Maleki et al. 2023b). They obtained a contrast ratio of 13.58 dB in an area of 86 μm^2. Askarian et al. (2022a) designed a PC-based structure including x-shaped resonators with nonlinear defects. An optical bias was used to case 00 and two ports were assigned to one input where the signals into these ports are assumed to be in-phase. The contrast ratio and the area were equal to 9.32 dB and 561 μm^2, respectively. All of the mentioned structures have no tuning feature for controlling optical signal while the fabrication errors affect greatly the performance. Therefore, the possibility of tuning some parameters in the decoder's structure helps to compensate for the mentioned errors. Rahmi et al. (2022) reported a 2-to-4 decoder including 4 nonlinear ring resonators. The structure operation was based on the dropping through the resonators. The contrast ratio was about 8.7 dB and the area was greater than 487 μm^2. Arunkumar et al. (2023) proposed some sequential resonant cavities and a reflector for dropping the incoming signal corresponding to the optical intensity. They obtained a contrast ratio of 22.4 dB and an area of 295 μm^2.

Different materials such as silicon, gallium arsenide, chalcogenide, and polystyrene have been employed in the described structures. These materials possess distinct properties, and their physical parameters typically remain constant with only slight variations in the presence of an electric field. Consequently, altering the properties of these materials after fabrication to enhance the performance of the structures is generally not feasible. In this research, a graphene-SiO$_2$ stack is utilized in a photonic crystal-based decoder to enable the tuning of wave transmission in waveguides. By manipulating the applied voltage to the graphene, the chemical potential, dielectric coefficient, absorption coefficient, and refractive index can be modified. This control over the properties allows for regulating the amount of light passing through the waveguides, facilitating the decoding operation. The present study employs a novel electro-optic decoder that incorporates a graphene-SiO$_2$ multilayer stack within photonic crystals. The stack enhances the interaction between light and the material, resulting in a pronounced resonance at the desired wavelength. This aspect proves valuable in achieving high-quality factors for filtering applications. The proposed structure is characterized by its fast response, compact size, and adjustability, making it advantageous for various applications.

Section 2 introduces the proposed switch along with the significance of the graphene stack. Moving on to Sect. 3, the simulation results for the decoder are presented. Finally, in the last section, a summary of the paper's findings is provided.

2 The electro-optic switch

The proposed switch in Fig. 1a utilizes two stacks to regulate the passage of light through the waveguide. This regulation is achieved by adjusting the chemical potential of the graphene layers. The switch is designed with a silicon waveguide, assuming 500 nm in width and 260 nm in height. It is positioned near two photonic crystal structures on a SiO_2 sub-
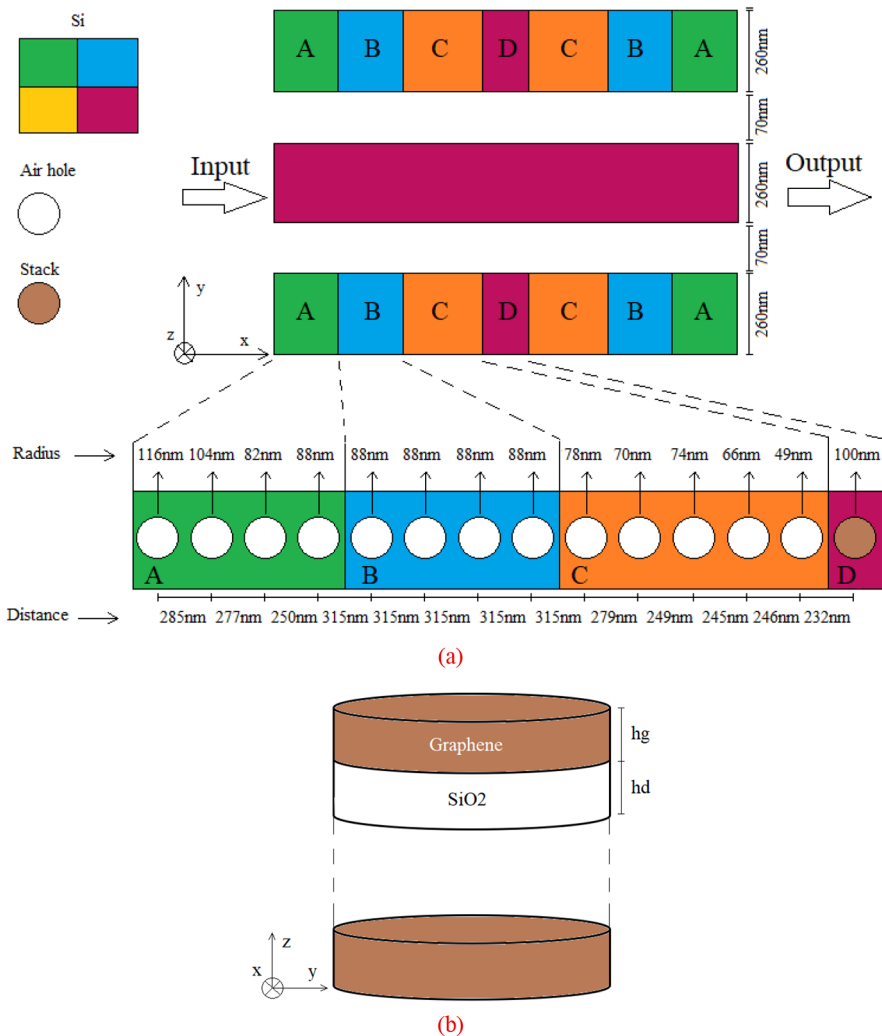

Fig. 1 (a) The electro-optic switch including a silicon waveguide and two one-dimensional photonic crystals, (b) the stack composed of graphene-SiO_2 layers

strate. As depicted in Fig. 1b, there is a graphene-SiO$_2$ stack at the center of the PC structure comprised of nine graphene layers, with a radius of 100 nm and a thickness of 1 nm. The stack is situated between SiO$_2$ layers. Surrounding the stack, there are air holes on both sides, denoted as parts A, B, and C. These holes exhibit symmetry with respect to the center of the cavity.

The cavities are positioned in proximity to the waveguide, allowing the incoming waves from the waveguide to be coupled into the cavities. The reflections from the holes in the structure function similarly to Bragg layers, determining the transmission of optical waves through the waveguide. By altering the graphene chemical potential, the permittivity of the graphene and stack can be modified, consequently affecting the interference in the photonic crystal cavity. This, in turn, influences the amount of wave transmission through the waveguide as it becomes dependent on the characteristics of graphene.

To simulate the propagation of optical waves, the finite difference time domain method is utilized. It calculates the magnetic and electric field components in both the spatial and temporal domains. In the simulation, the unit cells in all three dimensions have a length of Δu, equivalent to 0.2 nm. This value is much smaller than the wavelength (Sullivan 2000). Adhering to the Courant condition, the unit cell in the temporal domain (Δt) needs to be determined using Eq. (1) (Sullivan 2000):

$$c\Delta t \leq \frac{\Delta u}{\sqrt{3}} \tag{1}$$

The time step for the simulation is chosen as 0.0292 fs, taking into account the speed of light in vacuum, denoted as c. The boundary condition assumed in the simulation is the perfectly matched layer. The cavity exhibits characteristics similar to a frequency notch filter, primarily influenced by the total reflections due to the stack and different holes, as described by Maleki et al. (2020c). The obtained values for the central wavelength, bandwidth, and quality factor of the filter are 1492 nm, 0.03 nm, and 50,000, respectively. The quality factor is defined as the ratio of the central wavelength to the bandwidth. Furthermore, the extinction ratio is equal to 12.09 dB. This ratio is determined using the formula $10 \times \log(T_{max}/T_{min})$, where T_{min} and T_{max} represent the lowest and highest transmission factor, as explained by Maleki et al. (2020c). With a graphene chemical potential of 0.79 eV, a T_{max} of 96% and a T_{min} of 5.9% are achieved, resulting in an extinction ratio close to 12.09 dB. To calculate the transmission factor $T(\omega)$, which accounts for the cavity's proximity to the silicon waveguide, the model of transfer matrix, as outlined in Xu et al. (2015) findings, is employed.

$$T(\omega) = \left| \frac{S_{2-}}{S_{1+}} \right|^2 = \frac{4\tau_1\tau_2}{(\omega - \omega_0)^2 + (\tau_r + \tau_a + \tau_1 + \tau_2)^2} \tag{2}$$

S_{1+} and S_{2-} are the amplitudes of the reflective input and output fields, respectively. τ_1 and τ_2 denote the rates of coupling at the incoming and outcoming, while ω_0 represents the resonant frequency. τ_r and τ_a correspond to the rates of radiation loss and absorption in the photonic crystal. The graphene-SiO$_2$ stack allows for the manipulation of the graphene chemical potential by applying an electric field. Additionally, adjusting the number of graphene layers modifies the interaction between the incident light and the stack. This variation

is attributed to the stack's dielectric constant, which is mathematically described using the theory of effective medium, specifically in Eq. 3, as presented by Yadav et al. (2016).

$$\epsilon_{||} = \epsilon_{d} + \frac{j\sigma_{g}(\omega)}{\omega\epsilon_{0}h_{d}} \tag{3a}$$

$$\epsilon_{\perp} = \epsilon_{d} \tag{3b}$$

The permittivity components parallel and perpendicular to the horizontal plane are denoted as ε|| and ε⊥, respectively. In Fig. 1b, the graphene layers are arranged with SiO_2 layers separating them. The SiO_2 layers have a thickness of h_d=25 nm and a permittivity of ε_d=2.25. The angular frequency is represented by ω, and ε_0 symbolizes the permittivity of the vacuum. For electrical considerations, the surface conductivity of graphene monolayer (σ_g) is treated as a thin sheet (Su et al. 2015).

In Fig. 2, the variations in the imaginary and real parts of the dielectric constant for the stacked arrangement are presented in relation to the chemical potential per graphene layer at a wavelength of 1492 nm. It is observed that as the graphene chemical potential (or Fermi level) increases, the real part of ε|| initially rises and then decreases (as shown in Fig. 2a). This behavior aligns with the general characteristics of graphene, as demonstrated in the research conducted by Novoselov et al. (2012). Additionally, the imaginary part of ε|| experiences a rapid decrease within the range of 0.4 eV to 0.6 eV of μ_c and undergoes gradual changes in other ranges (see Fig. 2b). This indicates that for μ_c>0.4 eV, an increase in the chemical potential leads to a sharp decline in the imaginary part of the index for the stack. This phenomenon can be attributed to the Pauli exclusion principle. As the Fermi energy level or chemical potential increases, according to the mentioned principle, additional electron transitions to the conduction band are restricted, and valence band electrons are incapable of absorbing the incident photons. Consequently, absorption reduces as the chemical potential increases, resulting in graphene demonstrating transparency to light illumination (Jonghwan et al. 2012).

Figure 3 illustrates the effect of changing the chemical potential of graphene on wave transmission within the waveguide. When the chemical potential surpasses 0.4 eV, the cav-
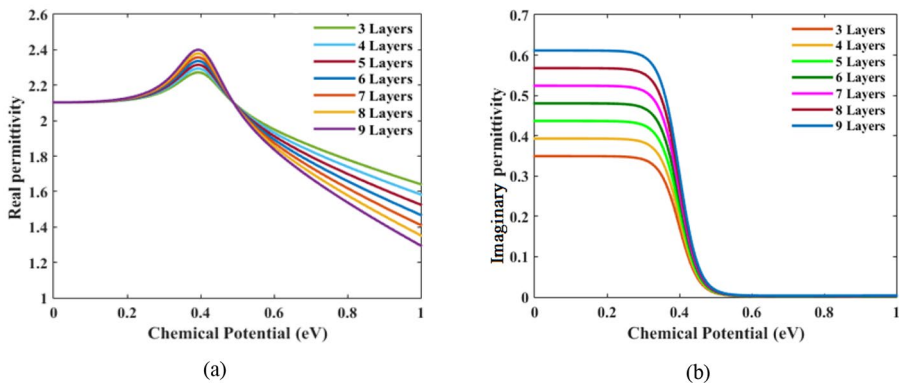

(a)   (b)

Fig. 2 (**a**) The real part and (**b**) the imaginary part of the parallel component of the stack's permittivity in terms of chemical potential for different numbers of graphene layers

ity resonance in the photonic crystal adversely affects the transmitted light, leading to the formation of a nearly complete stopband during the resonant wave. Conversely, for chemical potentials below 0.4 eV, the imaginary component of the stack's refractive index enhances the absorption coefficient of light within the cavity, thereby mitigating its destructive effects. Consequently, the amplitude of the light output from the device amplifies along the cavity resonance wavelength. This suggests that modifying the chemical potential enables the achievement of a switching operation. Figure 3a and b, and 3c exhibit the variation in light transmission for the chemical potential from 0.1 eV to 0.9 eV and the varying number of graphene layers within a stack periodicity. As the number of graphene layers in the spatial periodicity increases from one to three, there is a corresponding decrease in the central wavelength, as demonstrated in Fig. 3d.

Assuming the changes in the stack's chemical potential as the perturbation and keeping the electric field distribution fixed, the equation proposed by Jonghwan et al. (2012) provides a means to determine the alterations in the central wavelength of the light signal.

$$\frac{\lambda_0 - \lambda}{\lambda_0} \approx \frac{\iiint_V \left(\Delta\epsilon |E_0|^2 + \Delta\mu |H_0|^2 \right) dV}{\iiint_V \left(\epsilon |E_0|^2 + \mu |H_0|^2 \right) dV} \tag{4}$$
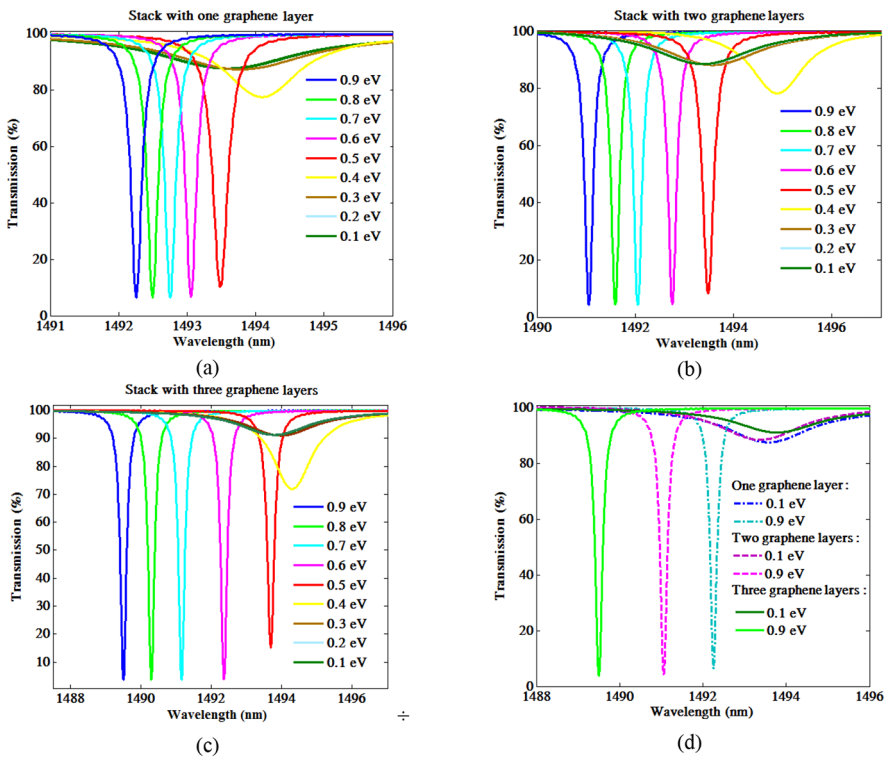

Fig. 3 The wave transmission in terms of the graphene chemical potential and wavelength for the stack with (**a**) one, (**b**) two, and (**c**) three graphene layers, (**d**) the transmission efficiency versus the wavelength for different graphene layers and the chemical potential of 0.1 eV and 0.9 eV

where λ_0, H_0, and E_0 represent the resonance wavelength in the PC cavity, magnetic field, and electric field intensities before the perturbation, respectively. On the other hand, λ represents the resonance wavelength after the perturbation. $\Delta\varepsilon$ and $\Delta\mu$ denote the magnitudes of the changes in the dielectric constant and magnetic permeability coefficient associated with the perturbation. Figure 2 shows that for chemical potentials exceeding 0.4 eV, the real part of the stack decreases, resulting in an enhancement of the resonance wavelength (Baba et al. 2003; Emani et al. 2014).

Regarding the potential for wavelength tuning, various studies have explored this concept. For instance, Yan et al. (2012) employed a graphene-insulator stack in a silicon-on-insulator structure to manipulate the transmission of notch filters. They successfully demonstrated tuning capabilities for frequencies lower than 1.2 THz. Zain et al. (2008) focused on designing and fabricating PC cavities for improving the quality factor in notch filters, utilizing the holes to enable adjusting the wavelength around 1.5 μm. Phare et al. (2015) introduce a structure for modulation operations, achieving wavelength tuning specifically at 1570 nm. Similarly, Pan et al. (2015) put forward a one-dimensional photonic crystal-based cavity with incorporated air holes. They utilized a graphene layer to modulate its operation and calculate the transmission at a span of wavelength. Their findings revealed a variation of approximately one nanometer around 1.55 μm when altering the chemical potential.

The relationship between the bias voltage and the graphene chemical potential (μ_c) can be expressed through the following equation (Maleki et al. 2023c):

$$\mu_c = \hbar v_F \sqrt{\pi\left(n_s + \frac{C\,|V|}{q}\right)} \tag{5}$$

The equation defines the intrinsic carrier concentration (n_s) for the given stack, where v_F represents the Fermi velocity of graphene, q is the electron charge, V denotes the bias voltage, and C represents the effective capacitance per unit area. This definition is derived from the research conducted byHaddadan and Soroosh (2023).

$$n_s = \frac{\epsilon(\omega)}{qh_d}V \tag{6}$$

The simulation results indicated that the extent of transmission using the silicon waveguide relies on the graphene chemical potential utilized in the stack. Specifically, for certain wavelengths, the transmission efficiency in the waveguide is reduced by 3%. This means that the light transmission coefficient through the waveguide adjacent to the photonic crystal cavity is possibly controlled by adjusting the graphene chemical potential in the stack. This capability to tune transmission by modifying the chemical potential is a promising finding with potential applications in optical device design. As a consequence, in the subsequent section, a 1-to-2 decoder will be designed based on two different chemical potentials: 0.1 eV and 0.9 eV.

Fig. 4 The proposed structure for
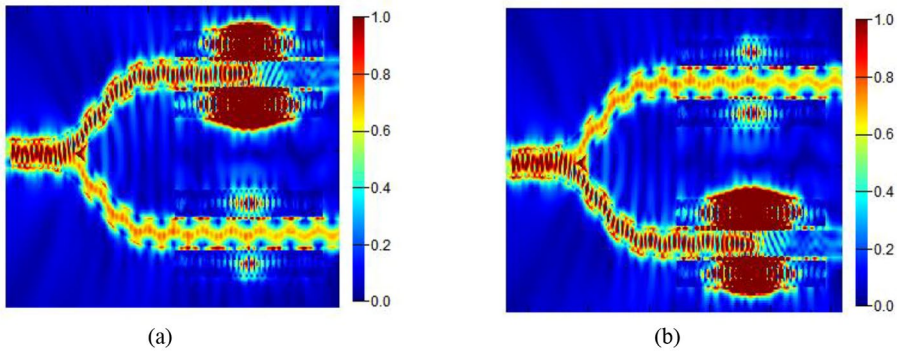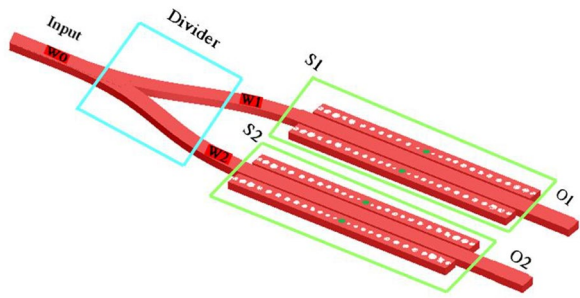1-to-2 electro-optic decoder

(a)　　　　　　　　　　　　　　　　　(b)

Fig. 5 The wave propagation inside the proposed structure for (**a**) $\mu_{c1}=0.9$ eV, $\mu_{c2}=0.1$ eV (**b**) $\mu_{c1}=0.1$ eV, $\mu_{c2}=0.9$ eV
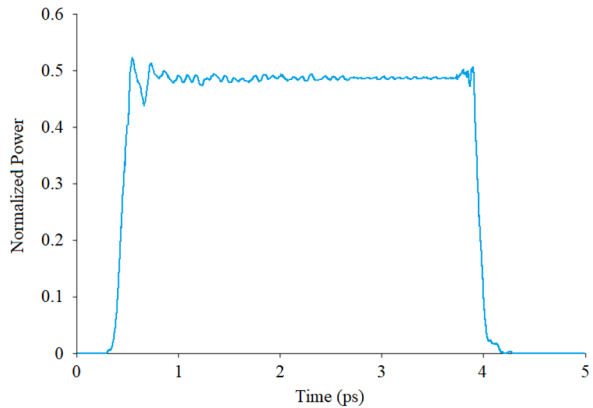
3 The proposed decoder

Figure 4 depicts the proposed structure utilizing the electro-optic switch. The decoder is comprised of a divider and two switches, S1 and S2. A 1492 nm optical signal enters through the input port and is guided to either output ports O1 or O2 via waveguides W0, W1, and W2. The input port is connected to an optical divider with 5 μm in length and 2 μm in width. Adjacent to waveguides W1 and W2, there are two photonic crystal resonant cavities responsible for regulating the transmission of light waves through the waveguides using graphene-SiO$_2$ stacks. As mentioned in Sect. 2, when the chemical potential of graphene is tuned to 0.1 eV, the light waves are transmitted through either waveguide W1 or W2. However, if $\mu_{c1}=\mu_{c2}=0.9$ eV, which denotes the chemical potentials of graphene at switches S1 and S2 respectively, the waves are not allowed to pass through waveguides W1 and W2.

To assess the decoder's performance, one can initially consider the scenario where $\mu_{c1}=0.9$ eV and $\mu_{c2}=0.1$ eV. In Fig. 5a, we observe that due to the resonance occurring in the cavities of S1, only a small portion of the incoming power from W0 appears at port O1. Meanwhile, the optical waves pass through W0 and W2, ultimately reaching port O2. Consequently, O1 becomes switched OFF while O2 is switched ON. Turning attention to Fig. 5b, when $\mu_{c1}=0.1$ eV and $\mu_{c2}=0.9$ eV, the incoming waves are guided through waveguide W1 towards output port O1, whereas switch S2 prevents the transmission of waves. Consequently, O1 is switched ON while O2 remains switched OFF.

Table 1 The obtained results of the proposed decoder

Chemical potential		Switch		Output Port			
μ_{c1} (eV)	μ_{c2} (eV)	S1	S2	Normalized Power (%)		Logic	
				O1	O2	O1	O2
0.9	0.1	OFF	ON	6.2	48	0	1
0.1	0.9	ON	OFF	48	6.2	1	0

Fig. 6 The time response of the decoder for an optical pulse with a duration of 3.8 ps. The graphene chemical potential equals 0.9 eV in order to allow SPP transmission through the plasmonic waveguide

According to Figs. 3 and 5, the manipulation of the graphene's chemical potential in the stack allows for control over the transmitted signal from the input to the outputs. The obtained analysis of the proposed device is briefly given in Table 1. For μ_{c1} = 0.1 eV and μ_{c2} = 0.9 eV, the table indicates that the normalized power at ports O1 and O2 is 48% and 6.2% respectively. Similarly, when μ_{c1} and μ_{c2} are adjusted to 0.9 eV and 0.1 eV respectively, the normalized power at O1 and O2 becomes 6.2% and 48% respectively.

Figure 6 shows the time response for an optical pulse with a width of 3.8 ps. The chemical potential of graphene is set to be 0.9 eV where surface plasmon polaritons are allowed to transmit through the plasmonic waveguides. First, the structure is illuminated for a duration of 3.8 ps. In this case, SPPs are excited toward the output port. Due to the symmetry of the structure for O1 and O2, the simulation results are similar at O1 and O2. After 3.8 ps, light is cut off and the terahertz waves vanish. The rise and fall times are equal to 517 fs and 196 fs, respectively. The rise time is equal to the time required for the signal to reach 90% of the final value. The fall time is the time when the signal drops by 10%.

The simulation results show that the designed decoder effectively directs and guides the incoming waves toward the output ports using switches S1 and S2. The intensity of light that travels through waveguides W1 and W2 is regulated by modifying the graphene chemical potential. Equation 5 indicates that μ_c can be properly adjusted by using a bias voltage.

Several studies have explored the feasibility of fabricating structures similar to the proposed design. Zein et al. (2008) successfully designed and fabricated a silicon-on-insulator-based one-dimensional photonic crystal cavity, incorporating air holes ranging from 65.5 to 171 nm in radius. They utilized a 200 nm layer of hydrogen silsesquioxane negative tone resist to define the waveguide pattern. Through the use of a Vistec VB6 machine operating at 100 KeV energy with proximity correction and a base dose of 1500 μC/cm^2, the cavi-

ties with different air holes were fabricated using a single-step direct-write electron-beam lithography. Similarly, Yan et al. (2012) accomplished the fabrication and characterization of various graphene/insulator stacks for notch filters, achieving an extinction ratio of 9.5 dB. The device fabrication involved some stages such as coating a polymer buffer, depositing wafer-scale graphene, graphene doping, and patterning into the desired structures. Considering these studies, there is reason to be optimistic about the feasibility of fabricating the proposed decoder.

While there have been reports on all-optical decoders in recent years, no structures utilizing electro-optic effects have been proposed for such decoders to date. In previous studies, the output parameters of the designed devices could not be adjusted post-fabrication. However, the proposed structure in this research is an electro-optic device, offering the advantage of adjustability after fabrication by changing the graphene chemical potential.

Table 2 demonstrates that the proposed structure exhibits a higher contrast ratio compared to Khosravi et al. 2017; Daghooghi et al. 2017, 2018b; Rahmi et al. (2022). The contrast ratio is calculated using the formula 10×log(P1/P0), where P1 and P0 represent the margins of logic 1 and 0, respectively. Generally, a higher contrast ratio makes a more possible to distinguish logic 0 and logic 1. As shown in Table 2, the area of the designed structure is smaller than 100 μm^2 crucial for use in the optical integrated circuits. The proposed structure is more compact than some works utilizing the ring resonators (Serajmohammadi et al. 2015; Alipour-Banaei et al. 2015; Mehdizadeh et al. 2016b; Moniem 2016; Khosravi et al. 2017; Daghooghi et al. 2017, 2018a, b; Maleki et al. 2020c; Rahmi et al. 2022; Arunkumar et al. 2023). Although Maleki et al. (2020b; 2020c) have presented a compact structure for optical decoders, no tuning of the structure after fabrication has remained a challenge. Using graphene can be considered as a solution to overcome the mentioned challenge because the complex refractive index of graphene changes in response to altering the chemical potential. Changing the refractive index results in the variation of real and imaginary parts of the refractive index. The real part and imaginary part are attributed to the optical confinement

Table 2 Comparison of the obtained results in this work with those in other works

Reference	Tunability	Area (μm^2)	Contrast Ratio (dB)
Serajmohammadi et al. 2015	No	267	12.79
Alipour-Banaei et al. 2015	No	611.7	not reported
Mehdizadeh et al. 2016b	no	1823	not reported
Moniem 2016	No	1520	not reported
Khosravi et al. 2017	No	1228	3.37
Daghooghi et al. 2017	no	1854.4	5.68
Salimzadeh et al. 2018	No	Not reported	9.29
Daghooghi et al. 2018a	No	368	9.95
Daghooghi et al. 2018b	no	380.25	5.44
Daghooghi et al. 2019	No	288	13.12
Maleki et al. 2019	No	90	not reported
Maleki et al. 2020b	No	76	13.52
Maleki et al. 2020c	no	110	13.42
Askarian 2022a	No	561	9.32
Rahmi et al. 2022	No	487.07	8.6
Arunkumar et al. 2023	No	295	22.4
Maleki et al. 2023b	No	86	13.58
This Work	Yes	99	8.89

and loss, respectively. Depending the stack's refractive index on the bias voltage makes a possibility to tune the optical confinement and transmission. This feature is the main advantage of the proposed device in comparison to other works. Furthermore, a contrast ratio of 8.89 dB and an area of 99 μm^2 demonstrate that the designed decoder can be used in different optical applications.

4 Conclusion

This paper introduces a 1-to-2 optical decoder composed of two electro-optic switches. Each switch in the structure utilizes photonic crystal-based cavity resonators with a silicon waveguide, positioned 70 nm apart. Within the photonic crystal, air holes are used, and a graphene-SiO_2 stack is placed at the cavity's center to establish resonance. The stack consists of nine monolayers of graphene sandwiched between layers of SiO_2, with a radius of 100 nm. Simulation results illustrate that the decoder can transmit 48% of the incoming power to the output port for logic 1, while 6.2% of the input power appears at the output port for logic 0. Consequently, the contrast ratio of the decoder is calculated to be 8.89 dB. The compact size of this designed decoder is a critical feature, distinguishing it from previous works and making it suitable for optical integrated circuits.

Data availability No datasets were generated or analysed during the current study.

Declarations

Ethical approval Not applicable.

Competing interests The authors declare no competing interests.

Conflict of interest The authors declare no conflicts of interest.

References

Alipour-Banaei, H., Mehdizadeh, F., Serajmohammadi, S., Hassangholizadeh-Kashtiban, M.: A 2*4 all optical decoder switch based on photonic crystal ring resonators. J. Mod. Opt. **62**, 430–434 (2015). https://doi.org/10.1080/09500340.2014.957743

Arunkumar, R., Robinson, S.: Realization of an all-optical 2* 4 decoder based on a two-dimensional photonic crystal. Opt. Quant. Electron. **55**, 570 (2023). https://doi.org/10.1007/s11082-023-04855-0

Askarian, A., Akbarizadeh, G.: A novel proposal for all optical 2× 4 decoder based on photonic crystal and threshold switching method. Opt. Quant. Electron. **54**, 1–15 (2022a). https://doi.org/10.1007/s11082-021-03443-4

Askarian, A., Akbarizadeh, G., Fartash, M.: A novel proposal for all optical half-subtractor based on photonic crystals. Opt. Quant. Electron. **51**, 1–9 (2019). https://doi.org/10.1007/s11082-019-1978-6

Askarian, A.: All optical half subtractor based on linear photonic crystals and phase shift keying technique. J. Opt. Commun. **00001015152021a0095** (2021b). https://doi.org/10.1515/joc-2021-0095

Askarian, A.: Compact and ultrafast all optical 1-bit comparator based on wave interference and threshold switching methods. J. Opt. Commun. **000010151520200311** (2021a). https://doi.org/10.1515/joc-2020-0311

Askarian, A.: Design and implementation of all optical 4× 2 encoder based on 2D-PhC platform and optical Kerr effect. Opt. Quant. Electron. **55**, 822 (2023b). https://doi.org/10.1007/s11082-023-04957-9

Askarian, A.: Design and implementation of all optical OR and NOR gates based on PhC structure and nonlinear Kerr effect. J. Opt. Commun. (2022b). https://doi.org/10.1515/joc-2022-0041

Askarian, A., Parandin, F.: Investigations of all-optical gates based on linear photonic crystals using the PSK technique and beam interference effect. Electromagnetics. **43**, 291–308 (2023a). https://doi.org/10.1080/02726343.2023.2244829

Askarian, A., Parandin, F.: Numerical analysis of all optical 1-bit comparator based on PhC structure for optical integrated circuits. Opt. Quant. Electron. **55**, 419 (2023c). https://doi.org/10.1007/s11082-023-04552-y

Askarian, A.: Performance analysis of all optical 2× 1 multiplexer in 2D photonic crystal structure. J. Opt. Commun. (2021c). https://doi.org/10.1515/joc-2021-0235

Baba, T., Shiga, M., Inoshita, K., Koyama, F.: Carrier plasma shift in GaInAsP photonic crystal point defect cavity. Electron. Letter. **39**, 1518–1516 (2003). https://doi.org/10.1049/el:20030930

Daghooghi, T., Soroosh, M., Ansari-Asl, K.: A low-power all Optical Decoder based on Photonic Crystal Nonlinear Ring resonators. J. Mod. Opt. **65**, 1415–1422 (2018a). https://doi.org/10.1016/j.ijleo.2018.08.090

Daghooghi, T., Soroosh, M., Ansari-Asl, K.: A novel proposal for all-optical decoder based on photonic crystals. Photon Netw. Commun. **35**, 335–341 (2017). https://doi.org/10.1007/s11082-021-03443-4

Daghooghi, T., Soroosh, M., Ansari-Asl, K.: Slow light in ultra compact photonic crystal decoder. Appl. Opt. **58**, 2050–2057 (2019). https://doi.org/10.1364/AO.58.002050

Daghooghi, T., Soroosh, M., Ansari-Asl, K.: Ultra-fast all-optical decoder based on nonlinear photonic crystal ring resonators. Appl. Opt. **57**, 2250–2257 (2018b). https://doi.org/10.1364/AO.57.002250

Emani, N.K., Chung, T.F., Kildishev, A.V., Shalaev, V.M., Chen, Y.P., Boltasseva, A.: Electrical modulation of Fano resonance in plasmonic nanostructures using graphene. Nano Letter. **14**, 78–82 (2014). https://doi.org/10.1021/nl403253c

Foroughifar, A., Saghaei, H., Veisi, E.: Design and analysis of a novel four-channel optical filter using ring resonators and line defects in photonic crystal microstructure. Opt. Quant. Electron. **53**, 101 (2021). https://doi.org/10.1007/s11082-021-02743-z

Haddadan, F., Soroosh, M., Alaei-Sheini, N.: Designing an electro-optical encoder based on photonic crystals using the graphene-Al2O3 stacks. Appl. Opt. **59**, 2179–2185 (2020). https://doi.org/10.1364/AO.386248

Haddadan, F., Soroosh, M.: A new proposal for 4-to-2 Optical Encoder using Nonlinear Photonic Crystal Ring resonators. Int. J. Opt. Photonics. **13**, 119–126 (2019b). https://doi.org/10.29252/ijop.13.2.119

Haddadan, F., Soroosh, M.: Design and simulation of a subwavelength 4-to-2 graphene-based plasmonic priority encoder. Opt. Laser Technol. **157**, 108680 (2023). https://doi.org/10.1016/j.optlastec.2022.108680

Haddadan, F., Soroosh, M.: Low-power all-optical 8-to-3 encoder using photonic crystal-based waveguides. Photon Netw. Commun. **37**, 83–89 (2019a). https://doi.org/10.1007/s11107-018-0795-3

Hosseinzadeh Sani, M., Ghanbari, A., Saghaei, H.: An ultra-narrowband all-optical filter based on the resonant cavities in rod-based photonic crystal microstructure. Opt. Quant. Electron. **52**, 295 (2020). https://doi.org/10.1007/s11082-020-02418-1

Jonghwan, K., Son, H., Cho, D.J., Geng, B., Regan, W., Shi, S., Kim, K., Zettl, A., Shen, Y.R., Wang, F.: Electrical control of optical plasmon resonance with graphene. Nano Letter. **12**, 5598–5602 (2012). https://doi.org/10.1021/nl302656d

Khosravi, S., Zavvari, M.: Design and analysis of integrated all-optical 2×4 decoder based on 2D photonic crystals. Photon Netw. Commun. **35**, 122–128 (2017). https://doi.org/10.1007/s11107-017-0724-x

Makvandi, M., Maleki, M.J., Soroosh, M.: Compact all-optical encoder based on silicon photonic crystal structure. J. Appl. Res. Electr. Eng. **1**, 1–7 (2020). https://doi.org/10.22055/jaree.2020.31442.1007

Maleki, M.J., Mir, A., Soroosh, M.: Design and analysis of a new compact all-optical full-adder based on photonic crystals. Optik. **227**, 166107 (2021b). https://doi.org/10.1016/j.ijleo.2020.166107

Maleki, M.J., Mir, A., Soroosh, M.: Designing an ultra-fast all-optical full-adder based on nonlinear photonic crystal cavities. Opt. Quant. Electron. **52**, 196 (2020a). https://doi.org/10.1007/s11082-020-02311-x

Maleki, M.J., Mir, A., Soroosh, M.: Ultra-fast all-optical full-adder based on nonlinear photonic crystal resonant cavities. Photon Netw. Commun. **41**, 93–101 (2021a). https://doi.org/10.1007/s11107-020-00917-5

Maleki, M.J., Soroosh, M., Akbarizadeh, G.: A compact high-performance decoder using the resonant cavities in photonic crystal structure. Opt. Quant. Electron. **55**, 852 (2023b). https://doi.org/10.1007/s11082-023-05139-3

Maleki, M.J., Soroosh, M., Akbarizadeh, G.: A subwavelength graphene surface plasmon polariton-based decoder. Diam. Relat. Mater. **134**, 109780 (2023c). https://doi.org/10.1016/j.diamond.2023.109780

Maleki, M.J., Soroosh, M.: A novel proposal for performance improvement in two-dimensional photonic crystal-based 2-to-4 decoders. Laser Phys. **30**, 076203 (2020b). https://doi.org/10.1088/1555-6611/ab9089

Maleki, M.J., Soroosh, M.: An ultra-fast all-optical 2-to-1 digital multiplexer based on photonic crystal ring resonators. Opt. Quant. Electron. **54**, 397 (2022b). https://doi.org/10.1007/s11082-022-03781-x

Maleki, M.J., Soroosh, M.: Design and simulation of a compact all-optical 2-to-1 digital multiplexer based on photonic crystal resonant cavity. Opt. Quant. Electron. **54**, 818 (2022a). https://doi.org/10.1007/s11082-022-04235-0

Maleki, M.J., Soroosh, M., Mir, A.: Improving the performance of 2-to-4 optical decoders based on photonic crystal structures. Crystals. **9**, 635 (2019). https://doi.org/10.3390/cryst9120635

Maleki, M.J., Soroosh, M., Mir, A.: Ultra-fast all-optical 2-to-4 decoder based on a photonic crystal structure. Appl. Opt. **59**, 5422–5428 (2020c). https://doi.org/10.1364/AO.392933

Maleki, M.J., Soroosh, M., Parandin, F., Haddadan, F.: Photonic crystal-based decoders: ideas and structures, in Recent Advances and Trends in Photonic Crystal Technology. IntechOpen, (2023a). https://doi.org/10.5772/intechopen.1002401

Mehdizadeh, F., Soroosh, M., Alipour-Banaei, H.: A novel proposal for optical decoder switch based on photonic crystal ring resonators. Opt. Quant. Electron. **48**, 20 (2016b). https://doi.org/10.1007/s11082-015-0313-0

Mehdizadeh, F., Soroosh, M., Alipour-Banaei, H.: Proposal for 4- to-2 optical encoder based on photonic crystals structure. IET Optoelectron. **11**, 29–35 (2017). https://doi.org/10.1049/iet-opt.2016.0022

Mehdizadeh, F., Soroosh, M.: Designing of all optical NOR gate based on photonic crystal. Indian J. Pure Appl. Phys. **54**, 35–39 (2016a). https://doi.org/10.56042/ijpap.v54i01.5678

Moniem, T.A.: All optical active high decoder using integrated 2D square lattice photonic crystals. J. Mod. Opt. **62**, 1643–1649 (2016). https://doi.org/10.1080/09500340.2015.1061061

Noori, M., Soroosh, M., Baghban, H.: Self collimation in photonic crystals: Applications and opportunities. Annalen Der Phys. **530**, 1700049 (2018). https://doi.org/10.1002/andp.201700049

Novoselov, K.S., Falko, V.I., Colombo, L., Gellert, P.R., Schwab, M.G., Kim, K.: A roadmap for graphene. Nature. **490**, 192–200 (2012). https://doi.org/10.1038/nature11458

Osgood, R., Meng, X.: Principles of Photonic Integrated Circuits: Materials, Device Physics. Guided Wave Design. Springer (2021). https://doi.org/10.1007/978-3-030-65193-0

Pan, T., Qiu, C., Wu, J., Jiang, X., Liu, B., Yang, Y., Zhou, H., Soref, R., Su, Y.: Analysis of an electro-optic modulator based on a grapheme silicon hybrid 1D photonic crystal nanobeam cavity. Opt. Express. **23**, 23358–23364 (2015). https://doi.org/10.1364/OE.23.023357

Parandin, F., Mahtabi, N.: Design of an ultra-compact and high-contrast ratio all-optical NOR gate. Opt. Quant. Electron. **53**, 666 (2021). https://doi.org/10.1007/s11082-021-03322-y

Parandin, F., Sheykhian, A., Askarian, A.: A novel design of an all-optical D flip-flop based on 2D photonic crystals. Microw. Opt. Technol. Lett. **66**, e34006 (2024). https://doi.org/10.1002/mop.34006

Phare, C.T., Lee, Y.H.D., Cardenas, J., Lipson, M.: Graphene electro-optic modulator with 30 GHz bandwidth. Nat. Photonics. **9**, 511–514 (2015). https://doi.org/10.1038/nphoton.2015.122

Rahmi, B., Badaoui, H., Abri, M.: Original architecture of an efficient all-optical 2×4 photonic crystals decoder based on nonlinear ring resonators. Opt. Quant. Electron. **54**, 676 (2022). https://doi.org/10.1007/s11082-022-04110-y

Salimzadeh, A., Alipour-Banaei, H.: A novel proposal for all optical 3 to 8 decoder based on nonlinear ring resonators. J. Mod. Opt. **65**, 2017–2024 (2018). https://doi.org/10.1080/09500340.2018.1489077

Serajmohammadi, S., Alipour-Banaei, H., Mehdizadeh, F.: All optical decoder switch based on photonic crystal ring resonator. Opt. Quant. Electron. **47**, 1109–1115 (2015). https://doi.org/10.1007/s11082-014-9967-2

Sullivan, D.M.: Electromagnetic Simulation Using the FDTD Method. Wiley-IEEE (2000)

Su, Z., Yin, J., Zhao, X.: Terahertz dual-band metamaterial absorber based on graphene/MgF2 multilayer structures. Opt. Express. **23**, 1679–1690 (2015). https://doi.org/10.1364/OE.23.001679

Xu, W., Zhu, Z.H., Liu, K., Zhang, J.F., Yuan, X.D., Lu, Q.S., Qin, S.Q.: Chip-integrated nearly perfect absorber at telecom wavelengths by graphene coupled with nanobeam cavity. Opt. Letter. **40**, 3256–3259 (2015). https://doi.org/10.1364/OL.40.003256

Yadav, A., Danesh, M., Zhong, L., Cheng, G.J., Jiang, L., Chi, L.: Spectral plasmonic effect in the nano-cavity of dye-doped nano sphere-based photonic crystals. J. Nanatechnol. **27**, 165703 (2016). https://doi.org/10.1088/0957-4484/27/16/165703

Yan, H., Li, X., Chandra, B., Tulevski, G., Wu, Y., Freitag, M., Zhu, W., Avouris, P., Xia, F.: Tunable infrared plasmonic devices using graphene/insulator stacks. Nat Nanotechnol. **7**, 330–334 (2012).

Zain, A.R.M., Johnson, N.P., Sorel, M., Rue, R.M.D.: Ultra high quality factor one dimensional photonic crystal/photonic wire micro cavities in silicon-on-insulator (SOI). Opt. Express. **16**, 12084–12089 (2008). https://doi.org/10.1364/OE.16.012084